

Superconductivity and magnetism in bilayer nickelates: itinerant perspective

Yi-Ming Wu,^{1,*} Tobias Helbig,^{1,†} Salahudin V. Smailagić,¹ Hao-Xin Wang,² Yijun Yu,^{3,4,5} Harold Y. Hwang,^{3,4} and Srinivas Raghu¹

¹*Leinweber Institute for Theoretical Physics, Stanford University, Stanford, CA 94305, USA*

²*Department of Physics, The Chinese University of Hong Kong, Sha Tin, New Territories, Hong Kong, China*

³*Stanford Institute for Materials and Energy Sciences,*

SLAC National Accelerator Laboratory, Menlo Park, CA 94025, USA

⁴*Department of Applied Physics, Stanford University, Stanford, CA 94305, USA*

⁵*Department of Physics, Fudan University, Shanghai 200438, China*

We study superconductivity and magnetism in bilayer nickelates from an itinerant perspective. Starting from a tight binding fit to recent ARPES measurements on compressively strained thin films, we incorporate the standard set of onsite repulsive interactions among partially filled e_g orbitals: intra-orbital U , inter-orbital U' , Hund's coupling J_H and a pair hopping J_P . We obtain the effective pairing interaction by dressing these bare interactions with particle-hole fluctuations via the RPA. In the strong Hund's coupling regime, we find that s -wave superconductivity and $(\pi/2, \pi/2)$ SDW order are the favored ground states. With weaker Hund's coupling, we find that d -wave pairing and (π, π) SDW are the leading ground states. Our results are qualitatively consistent with earlier DMRG studies, and point to the key role played by Hund's coupling in determining the nature of superconductivity and magnetism in this system.

I. INTRODUCTION

The bilayer nickelates are a newly discovered family of high- T_c superconductors that have been under intensive study in recent years. The bulk material becomes superconducting under high pressure with a transition temperature $T_c \approx 80\text{K}$ [1–6], and more recently, superconductivity with $T_c \approx 40\text{K}$ has been observed in compressively strained thin film samples [7–9]. As a function of pressure or compressive strain, the system undergoes a structural transition from a low pressure orthorhombic [10, 11] to nearly tetragonal system at high pressure/compressive strain. At ambient pressure or without compressive strain, superconductivity is absent; instead, spin stripe order with $\mathbf{Q} = (\pi/2, \pi/2)$ has been observed [12–19]. Such magnetic order is distinct from the conventional (π, π) Néel order observed for example in the La-based cuprate parent compound La_2CuO_4 [20, 21]. The microscopic origin of the spin stripe phase and its connection to superconductivity are actively being debated at present [22–63].

Recent APRES measurements [64–66] have shed some light on this issue and revealed that the low-energy fermions in $\text{La}_3\text{Ni}_2\text{O}_7$ have dominant contributions from the e_g subspace of $3d$ -orbitals: $d_{x^2-y^2}$ and d_{z^2} . In a recent theoretical study [67], we have shown that $\mathbf{Q} = (\pi/2, \pi/2)$ spin stripe order can stem from a sizable Hund's coupling J_H between the itinerant $d_{x^2-y^2}$ electrons and the more localized spins in the d_{z^2} orbitals. Furthermore, given the proximity of superconductivity to magnetism, it is likely that the scale of Hund's coupling relative to that of in-plane superexchange will significantly influence the pairing symmetry. Indeed, in Ref.

[67], we reported that interlayer singlet Cooper pairing was the dominant pairing tendency, which was stabilized by J_H , and which is equivalent to an s -wave paired state. In the case of $\text{La}_3\text{Ni}_2\text{O}_7$, recent experiments reported signatures of s -wave [68, 69] and d -wave [70] pairing, where a competition between the two is generically expected from the fermiology of the bilayer system [71]. From a theoretical perspective, proposals supporting s -wave pairing include studies using FRG [22, 72], DMRG [25, 67], mean-field theory [24, 37, 73–75] and the fluctuation-exchange approximation [76], while studies using t - J models found d -wave pairing similar to that in cuprates [36, 52, 77].

In this work, we investigate both superconductivity and magnetism in $\text{La}_3\text{Ni}_2\text{O}_7$ resulting from repulsive interactions including intra-orbital U , inter-orbital U' , Hund's coupling J_H and pair hopping $J_P \approx J_H$, with the goal of understanding how these microscopic interactions affect the pairing symmetry and the wave vector associated with magnetism. The effective pairing interaction V_{eff} is obtained by dressing these bare interactions with particle-hole excitations from spin and orbital fluctuations within the random phase approximation (RPA) [78–81]. We identify three characteristic s -wave pairing states that occur upon varying the microscopic interactions: a conventional fully gapped s -wave, a fully gapped s_{\pm} -wave, and a nodal s -wave that interpolates between them. Each requires a sizeable J_H defined relative to the scale of in-plane single electron tunneling. With weaker J_H , these s -wave states compete with two d -wave states of $x^2 - y^2$ (B_{1g}) and xy (B_{2g}) symmetry, with the B_{1g} occupying a larger region of the phase diagram. Through Hund's coupling, the interlayer hopping of the d_{z^2} orbitals induces an effective interlayer coupling in the $d_{x^2-y^2}$ sector. The d -wave pairing is stabilized only for small interlayer interaction and hence vanishingly small J_H . Based on these results, we speculate that s_{\pm} -wave pairing is the more likely superconducting ground state

* yimwu@stanford.edu

† helbig@stanford.edu

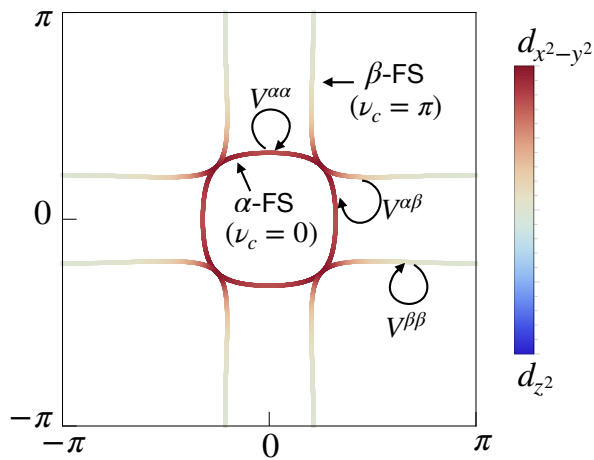


FIG. 1. Fermi surface of bilayer nickelate in the k_x - k_y plane from Eq. (1), with color encoding the orbital weight. Here the central pocket is the α -FS (bonding, $\nu_c = 0$), containing mainly contributions from the $d_{x^2-y^2}$ orbitals. The larger pocket surrounding (π, π) is the β -FS (anti-bonding, $\nu_c = \pi$), and has equal contributions from both orbitals near the BZ boundary. The effective intra-pocket interaction $V^{\alpha\alpha}$ and $V^{\beta\beta}$, and the inter-pocket $V^{\alpha\beta}$ are pictorially shown here, see Fig. 3 for details.

in $\text{La}_3\text{Ni}_2\text{O}_7$.

We then present results for magnetism within the RPA. We show that even at the non-interacting level, the bare spin and charge susceptibilities are peaked at $\mathbf{Q} = (\pi/2, \pi/2)$, and that this peak is further strengthened by sizeable Hund's coupling in the RPA. In the regime where Hund's coupling is weak, we find the dominant magnetism is a (π, π) antiferromagnet whose origin stems from a band with d_{z^2} character possessing a high density of states that occurs just below the Fermi level.

While these results are obtained in the limit where both orbital degrees of freedom are itinerant, they share some qualitative similarities with earlier DMRG studies [67], which incorporated stronger correlation effects and Mott physics. Both studies have found $(\pi/2, \pi/2)$ spin stripe order and pairing between electrons across the bilayer, and both resulted from a sizeable Hund's rule coupling. Despite the drastic differences in assumptions that underlie each of these techniques, such qualitative similarity points towards a robustness of these results that are likely inform experimental observations.

In the following, we present details of our model and method in Sec. II. In Sec. III, we discuss the resulting phase diagram and the corresponding gap symmetries as a function of the bare interactions, as well as the normal state magnetic ordering tendencies in the RPA total spin susceptibility. We point out key differences to previous weak-coupling studies, namely the importance of Hund's coupling and the non-degenerate nature of the e_g orbitals.

II. MODEL AND METHOD

Recent ARPES measurements [64–66] have indicated that the low energy fermions have dominant contributions from the e_g subspace of the Ni $3d$ -orbitals: $d_{x^2-y^2}$ and d_{z^2} . We model the kinetic part of the bilayer nickelates $\text{La}_3\text{Ni}_2\text{O}_7$ using a tight-binding fit to the ARPES data from Ref. [66]. We denote ψ_Z^\dagger, ψ_Z for d_{z^2} orbitals and ψ_X^\dagger, ψ_X for $d_{x^2-y^2}$ orbitals. This results in a spin-degenerate non-interacting Hamiltonian $H_0 = \sum_{\mathbf{k}, \sigma} \psi_{\sigma, \mathbf{k}}^\dagger \mathcal{H}_0(\mathbf{k}) \psi_{\sigma, \mathbf{k}}$ with $\psi_{\sigma, \mathbf{k}}^\dagger = (\psi_{X, \sigma, \mathbf{k}}^\dagger, \psi_{Z, \sigma, \mathbf{k}}^\dagger)$,

$$\mathcal{H}_0(\mathbf{k}) = \begin{pmatrix} \xi_X(\mathbf{k}) & T(\mathbf{k}) \\ T^\dagger(\mathbf{k}) & \xi_Z(\mathbf{k}) \end{pmatrix} \quad (1)$$

and matrix elements

$$\begin{aligned} \xi_X(\mathbf{k}) &= -2t_{1x} (\cos k_x + \cos k_y) - 4t_{2x} \cos k_x \cos k_y - \mu_d, \\ \xi_Z(\mathbf{k}) &= -t_z^\perp \cos \nu_c - 2t_{1z} (\cos k_x + \cos k_y) \\ &\quad - 4t_{2z} \cos k_x \cos k_y - \mu_f, \\ T(\mathbf{k}) &= -2t_{xz} (\cos k_x - \cos k_y) \\ &\quad - 2t_{xz}^\perp \cos \nu_c (\cos k_x - \cos k_y). \end{aligned} \quad (2)$$

The values of the parameters are taken from [66] and also given in Appendix A. We consider a single bilayer system with bonding and anti-bonding bands within the bilayer corresponding to $\nu_c = 0$ and $\nu_c = \pi$ respectively. These are the even ($e^{i\nu_c} = +1$) and odd components ($e^{i\nu_c} = -1$) under layer exchange in the c -axis bilayer splitting. To incorporate the spatial degrees of freedom, we define $\mathbf{k} \equiv (k_x, k_y, \nu_c)$. The Fermi surface (FS) obtained from diagonalizing $\mathcal{H}_0(\mathbf{k})$ is presented in Fig. 1. The bonding band ($\nu_c = 0$) is called α -FS and the anti-bonding band ($\nu_c = \pi$) β -FS. Note that in the model we use, the γ -pocket near (π, π) does not cross the Fermi level, consistent with ARPES data [66] measured on thin film samples.

To investigate the magnetic and superconducting instabilities in bilayer nickelates, we must include interactions via a Hamiltonian of the form $H = H_0 + H_I$. In a recent DMRG study [67], it was shown that the $\mathbf{Q} = (\pi/2, \pi/2)$ spin stripe order and a strong interlayer pairing tendency both stem from a sizable Hund's coupling J_H between the itinerant $d_{x^2-y^2}$ electrons and the localized spins in the d_{z^2} orbitals. In the itinerant perspective presented here, we allow for charge fluctuations to occur in both orbitals. Within this approach, one can ask whether a sizeable J_H is similarly needed to obtain the $\mathbf{Q} = (\pi/2, \pi/2)$ magnetic order and s -wave pairing. To investigate this question, we consider the Kanamori form [82] for the interacting part H_I which along with the intra-orbital Hubbard interaction U , inter-orbital onsite repulsion U' , pair hopping J_P , also includes Hund's cou-

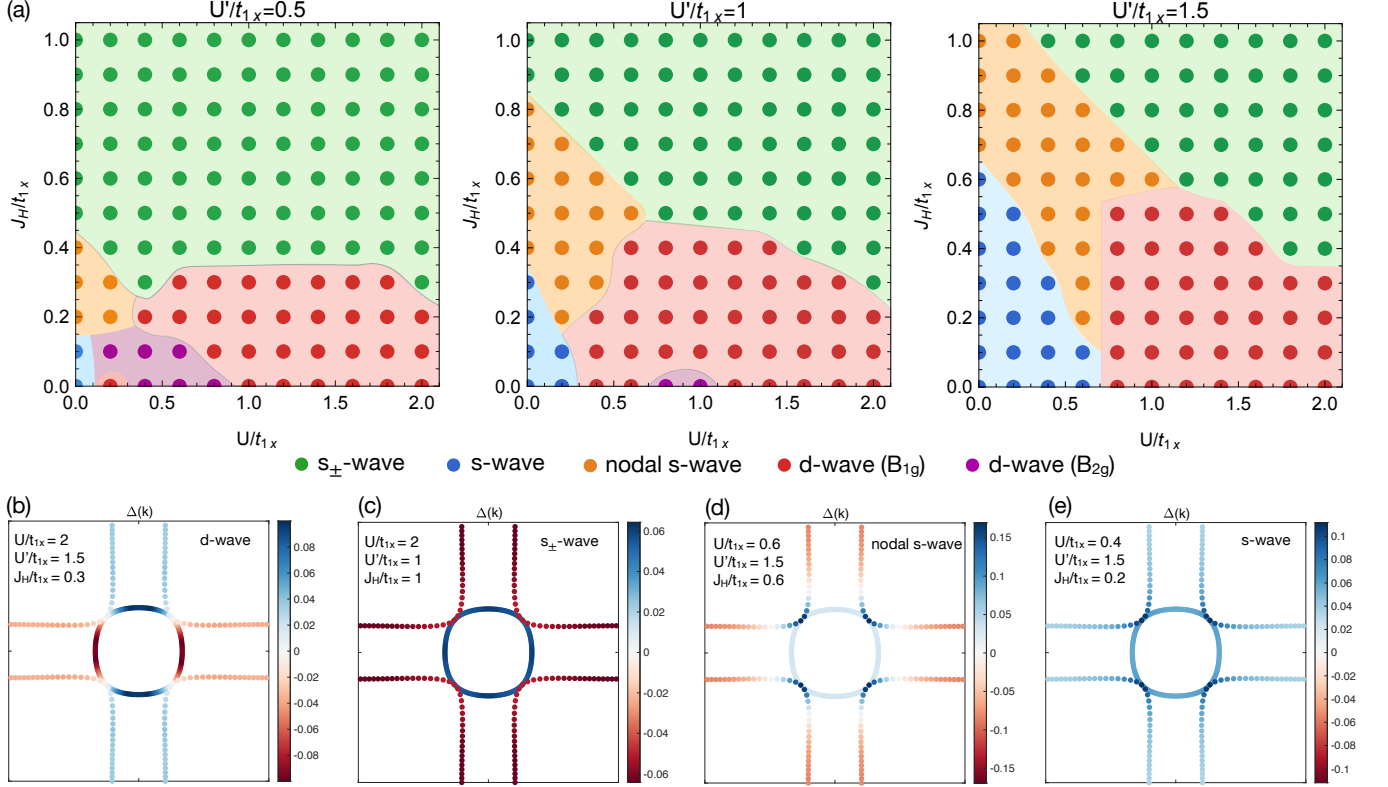


FIG. 2. (a) Phase diagram of the leading pairing symmetry in the parameter space $U'-U-J_H$. (b-e) Band basis projected gap function $\Delta(\mathbf{k})$ [see Eq. (4) and Appendix B] obtained at different parameters indicated in the plots. The value on the color bar shows the relative magnitude of the gap function. (b) d -wave gap function in the B_{1g} irrep with nodal points along the $\hat{x} \pm \hat{y}$ directions. (c) s_{\pm} -wave, (d) nodal s -wave and (e) conventional s -wave gap functions.

pling J_H . The Hamiltonian is

$$\begin{aligned}
 H_I = & U \sum_{\ell,i,a} n_{a,\ell,i,\uparrow} n_{a,\ell,i,\downarrow} + U' \sum_{a \neq b, \ell, i, \sigma, \sigma'} n_{a,\ell,i,\sigma} n_{b,\ell,i,\sigma'} \\
 & - J_H \sum_{\ell, i, \sigma, \sigma'} \psi_{X,\ell,i,\sigma}^\dagger \psi_{X,\ell,i,\sigma'} \psi_{Z,\ell,i,\sigma}^\dagger \psi_{Z,\ell,i,\sigma'} \\
 & + J_P \sum_{\ell, i} \left(\psi_{X,\ell,i,\uparrow}^\dagger \psi_{X,\ell,i,\downarrow}^\dagger \psi_{Z,\ell,i,\downarrow} \psi_{Z,\ell,i,\uparrow} + h.c. \right).
 \end{aligned} \tag{3}$$

Here i labels the position of each bilayer Ni-site, and $\ell = 1, 2$ labels the top and bottom layer. $a = X, Z$ is the orbital label, and σ is the spin label. The density is defined as $n_{a,\ell,i,\sigma} = \psi_{a,\ell,i,\sigma}^\dagger \psi_{a,\ell,i,\sigma}$.

In the case where the two e_g orbitals are degenerate, one may expect from a first order perturbation theory treatment of Coulomb matrix elements that $U' = U - 2J_H$ [83, 84]. Here, we treat these coupling as unconstrained *effective* interactions: we will treat U' , J_H and U independently, while keeping $J_P = J_H$.

We use RPA to explore the possible superconducting pairing instabilities of the effective pairing interaction which is the bare interaction dressed with particle-hole spin and orbital fluctuations and projected into the singlet Cooper channel. We further evaluate the spin sus-

ceptibility to shed light on the possible normal state magnetic ordering as a function of the Hund's coupling J_H . Within the RPA setup, which is detailed in Appendix A, we consider the geometric series of diagrams for both transverse and longitudinal spin and orbital fluctuations.

III. RESULTS

A. Superconductivity

We find the leading pairing instability as the solution to the linearized gap equation by the most negative eigenvalue of the symmetrized pairing kernel in the singlet channel, see Appendix B for details. Since the gap function $\Delta_{aa'}$ is a (2×2) -matrix given in orbital space, we project it to the band basis. Assuming it is the j -th band that is on the Fermi surface at each $\mathbf{k} \in \text{FS}$, the real-valued band basis projected gap function is given by

$$\Delta(\mathbf{k}) = \sum_{a,a'} u_{a,j}^*(\mathbf{k}) \Delta_{aa'}(\mathbf{k}) u_{a',j}^*(-\mathbf{k}) \tag{4}$$

where $a, a' \in (X, Z)$ and $u_{X,j}^*(\mathbf{k})$, $u_{Z,j}^*(\mathbf{k})$ are the complex conjugated components of the eigenvector of the j -th band of $\mathcal{H}_0(\mathbf{k})$.

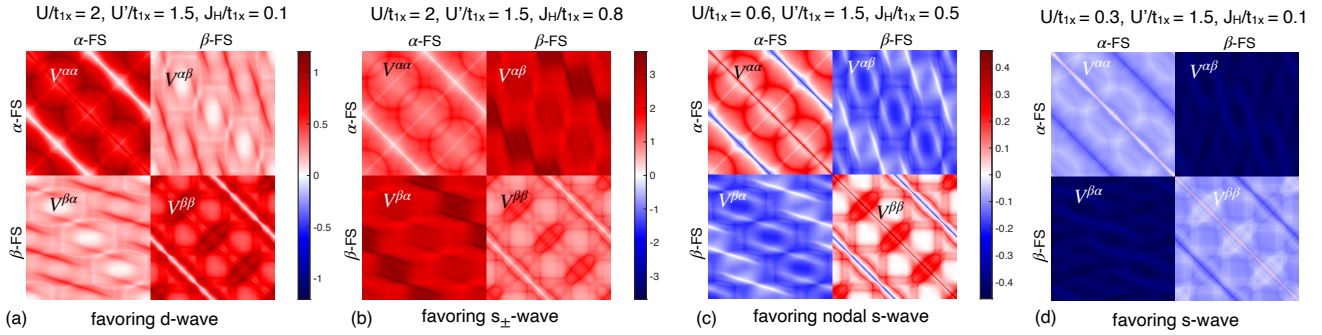


FIG. 3. Color maps of the effective interaction $[V_{\text{eff}}(\mathbf{k}, \mathbf{p})]_{XX,XX}$ between $d_{x^2-y^2}$ orbitals in the \mathbf{k} - \mathbf{p} plane. Since an equal number of points are sampled on the α -FS and on the β -FS, each plot is divided into four equal-size blocks: the intra-pocket interaction $V^{\alpha\alpha}$ and $V^{\beta\beta}$ and the inter-pocket interaction $V^{\alpha\beta} = [V^{\beta\alpha}]^T$. (a) When all of the interactions are repulsive and the intra-pocket $V^{\alpha\alpha}$, $V^{\beta\beta}$ dominate, the system favors a d -wave. (b) Instead, when the inter-pocket $V^{\alpha\beta}$ dominates in a fully repulsive interaction, the system favors a s_{\pm} -wave. (c) When $V^{\alpha\alpha}$ and $V^{\beta\beta}$ are repulsive but $V^{\alpha\beta}$ is attractive, the system favors a nodal s -wave. (d) When all these four interactions are attractive, the system favors a conventional s -wave.

In the following, we label each solution $\Delta(\mathbf{k})$ by the irreducible representation (irrep) of the crystalline symmetry group. Within the framework of Landau's theory of phase transitions, any two states Δ_1 and Δ_2 that belong to the same irrep can mix and coexist. In some cases, energetics will favor a state Δ_1 over Δ_2 even though both belong to the same irrep. This is relevant to the existence of “accidental nodes” on the gap function. In such cases, a small Δ_2 , although not forbidden, manifests itself at most as a small perturbation to the ground state. As we discuss below, this is precisely what occurs for various characteristic s -wave gap functions as a function of bare interaction strengths. Note that any putative phase boundaries between regions with dominant Δ_1 , say, and regions with dominant Δ_2 are crossovers, not sharp transitions. We request the reader to keep this basic framework in mind as we present the results below.

In Fig. 2(a) we show the phase diagrams of the leading pairing symmetries in the U - J_H plane for three different values of U' : $U'/t_{1x} = 0.5, 1$ and 1.5 . The phase diagram for each U' is plotted as a function of $U/t_{1x} \in [0, 2]$ and $J_H/t_{1x} \in [0, 1]$. We identify five competing pairing channels: fully gapped (nodeless) s_{\pm} -wave and s -wave, nodal s -wave, all of which belong to the same irrep, and d -wave states belonging to the B_{1g} and the B_{2g} irreps. Some representative examples of the band-projected gap function are shown in Fig. 2(b)-(e). For each of the examples of the band-projected gap function, we plot the effective pairing interaction $V_{\text{eff}}(\mathbf{k}, \mathbf{k}')$ between the $d_{x^2-y^2}$ orbitals projected onto the Fermi surface as color maps in Fig. 3.

For small Hund's coupling $J_H \lesssim U'/2$, the leading pairing instability occurs in the B_{1g} irrep, corresponding to a $x^2 - y^2$ -symmetry state, as shown in Fig. 2(b). The gap function has nodes along the diagonal directions ($\hat{x} \pm \hat{y}$) and is significantly larger on the α -Fermi surface than on the β -Fermi surface. The effective interaction between $d_{x^2-y^2}$ orbitals is purely repulsive [Fig. 3(a)] and is dominated by interactions $V^{\alpha\alpha}$, $V^{\beta\beta}$ within each Fermi

surface separately. In contrast, inter-pocket scattering $V^{\alpha\beta}$ between the α and β sheets is strongly suppressed. This hierarchy follows from the weak interlayer coupling of the $d_{x^2-y^2}$ orbitals at small J_H . Since the primary interlayer hopping process involves the d_{z^2} orbitals via the t_{\perp} hopping, the $d_{x^2-y^2}$ orbitals remain largely confined to individual layers. Consequently, pairing is predominantly intralayer, stabilizing a B_{1g} d -wave state. The nodal structure of this state is controlled by the momentum dependence of the repulsive interaction, dressed by spin fluctuations peaked at (π, π) as seen in the RPA spin susceptibility (blue) in Fig. 4. While this resembles the spin-fluctuation mechanism underlying d -wave pairing in cuprates, here the (π, π) fluctuations are enabled by the additional γ band close to the Fermi level.

Another d -wave pairing with xy -symmetry in the B_{2g} irrep is leading for vanishingly small J_H and $U \approx U'$. This d -wave pairing has nodes only on the α -FS along the \hat{x} - and \hat{y} -directions.

At large J_H , and approximately for $U + 2J_H > 1.6U'$, an s_{\pm} -wave state becomes the leading instability. This state is fully gapped, with opposite signs of the gap function on the α - and β -Fermi surfaces, as shown in Fig. 2(c). For large Hund's coupling, the interlayer processes active in the d_{z^2} channel generate an effective interlayer coupling in the $d_{x^2-y^2}$ sector. This renormalized interlayer interaction enhances scattering between the α and β Fermi surfaces. As reflected in Fig. 3(b), the effective interaction between the $d_{x^2-y^2}$ orbitals is therefore dominated by inter-pocket repulsion $V^{\alpha\beta}$, while intra-pocket contributions $V^{\alpha\alpha}$, $V^{\beta\beta}$ are suppressed. Such predominantly interband repulsion naturally favors a sign-changing yet fully gapped superconducting state, i.e., an s_{\pm} -pairing symmetry. The nature of the spin (and orbital) fluctuations that drive the s_{\pm} -wave pairing is also distinct from the d -wave case, as with large J_H the spin fluctuations carry momentum near $(\pi/2, \pi/2)$ instead of (π, π) . This can be seen from the calculated RPA total

spin susceptibility in blue in Fig. 4.

When $U + 2J_H \lesssim 1.6U'$ and $2J_H > U$, a distinct s -wave solution with eight nodal points on the β Fermi surface becomes dominant. An example of the corresponding gap function is shown in Fig. 2(d). Starting from the nodeless s_{\pm} -state, nodes first emerge along the diagonal directions and subsequently move toward the Brillouin zone boundary near $(0, \pi)$ and $(\pi, 0)$. Upon further reducing J_H and U , this nodal s -wave continuously crosses over into the conventional nodeless s -wave state realized near $J_H = U = 0$, as shown in Fig. 2(e). The nodal s -wave thus interpolates between the s_{\pm} and conventional s -wave limits. The evolution of the s -wave state is reflected in the effective interaction. In the parameter regime favoring the nodal s -wave [Fig. 3(c)], the interaction $V^{\alpha\beta}$ between the α - and β -Fermi surfaces becomes attractive, while the intra-pocket components $V^{\alpha\alpha}$, $V^{\beta\beta}$ remain repulsive. In contrast, in the conventional s -wave regime [Fig. 3(d)], the effective interaction is attractive for both inter- and intra-pocket processes, stabilizing a non-sign-changing s -wave gap. We note again that since these s -wave states all belong to the same irrep, there will be some admixture of the states; therefore, all nodes within the s -wave states are ‘‘accidental’’, and not protected by symmetry.

We note that in several previous studies the RPA method has also been applied to inspect the leading pairing symmetries [33, 49, 50, 65], with which our result reaches a qualitative agreement. However, as we commented above, the Fermi surface we analyze does not include the γ -pocket near the (π, π) BZ corner, which is mainly comprised of d_{z^2} orbitals. Thus, the agreement between our findings and previous studies imply the γ -pocket may be irrelevant to the pairing in bilayer nickelates. Finally we note that in our phase diagram Fig. 2(a) the regime for the leading s_{\pm} -wave pairing at $U + 2J_H > 1.6U'$ can be extended to even stronger interactions, and eventually reach agreement with the strong coupling results [25, 27, 67]. These results are in qualitative agreement with an earlier DMRG study on the role of Hund’s coupling both for superconductivity and magnetism.

B. Magnetism

In order to show how the Hund’s coupling J_H qualitatively affects magnetic ordering tendencies in the normal state, we present the results for the total spin susceptibility, calculated within RPA. The total spin- S_z susceptibility is obtained by

$$\chi_S^{\text{RPA}}(\mathbf{q}) = \sum_{a,b} \sum_{\alpha\gamma\beta\delta} [\chi^{\text{RPA}}(\mathbf{q})]_{aa\alpha\gamma;bb\beta\delta} \sigma_{\alpha\gamma}^z \sigma_{\delta\beta}^z, \quad (5)$$

where a, b are orbital indices and $\alpha, \beta, \gamma, \delta$ are spin indices. For comparison, we calculate the bare total spin susceptibility by summing over the orbital indices of the

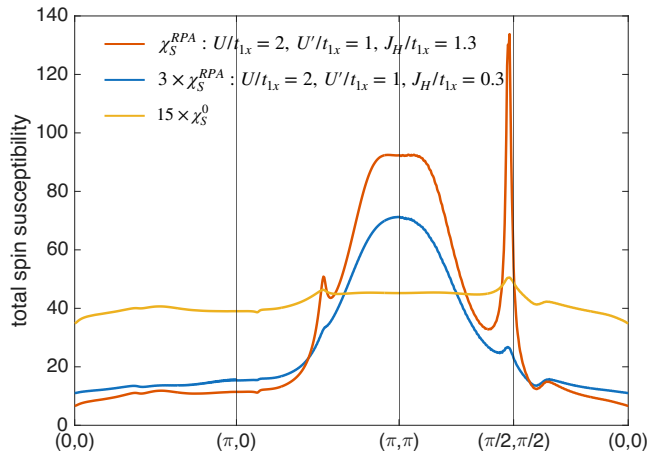


FIG. 4. Comparison of the RPA total spin susceptibility $\chi_S^{\text{RPA}}(\mathbf{q})$ and the bare total spin susceptibility $\chi_S^0(\mathbf{q})$, for \mathbf{q} along the path Γ -X-M- Γ in the BZ. $\chi_S^0(\mathbf{q})$ is shown in yellow. For $\chi_S^{\text{RPA}}(\mathbf{q})$, we fix U and U' and show two different values of J_H in blue and orange.

bare susceptibility $\chi^0(\mathbf{q})$ (defined in Appendix A) as

$$\chi_S^0(\mathbf{q}) = \sum_{a,b} [\chi^0(\mathbf{q})]_{aa,bb}. \quad (6)$$

In Fig. 4, we plot the bare and RPA total spin susceptibility along the path Γ -X-M- Γ for $\nu_c = \pi$. As depicted in yellow in Fig. 4, the bare $\chi_S^0(\mathbf{q})$ clearly peaks close to $\mathbf{Q} = (\pi/2, \pi/2)$, which we trace back to nesting effects between the α and β Fermi surface pockets along the diagonal direction in the BZ, see Appendix C.

With the blue and orange curves in Fig. 4, we further compare two different values of J_H of the RPA total spin susceptibility $\chi_S^{\text{RPA}}(\mathbf{q})$ while keeping all other parameters fixed. For a small J_H , $\chi_S^{\text{RPA}}(\mathbf{q})$ peaks at momentum (π, π) . The origin of this broad peak may be traced back to off-shell processes involving the γ -band. Since the γ -band is only slightly below the Fermi surface, scattering from and into these states, though algebraically suppressed, is still possible provided that interactions are strong enough. We find that among all the included RPA diagrams, the ‘transverse’ fluctuations which is comprised of ladders of V_1 do not change the maximum position of $\chi_S^0(\mathbf{q})$. It is the ‘longitudinal’ contributions which contain V_2 that tend to shift the maximum position to (π, π) [85]. At large enough J_H , $\chi_S^{\text{RPA}}(\mathbf{q})$ starts to peak near $(\pi/2, \pi/2)$. This is qualitatively consistent with the strong coupling theory of the $(\pi/2, \pi/2)$ order in bilayer nickelates in Ref. [67], where it is shown that a critical value of J_H is needed for the onset of this spin order (see Appendix C for details).

IV. DISCUSSION

Based on the results above, our key inference is that Hund's coupling influences both superconductivity and magnetism of bilayer nickelates in an essential way. The Hund's coupling favors s -wave states, and stabilizes magnetism with wave-vector $(\pi/2, \pi/2)$. By locking the d_{z^2} and $d_{x^2-y^2}$ orbital fluctuations together, the Hund's coupling favors a high spin state, which in turn influences the magnetic ordering tendencies. Furthermore, when J_H couples the d_{z^2} and $d_{x^2-y^2}$ orbital fluctuations, it *induces* an interlayer interaction in the $d_{x^2-y^2}$ sector from the *intrinsic* interlayer coupling of the d_{z^2} orbitals. In this way, Hund's rule, as well as the bilayer geometry crucially affect pairing.

We conclude with some broader implications of our findings. In previous work [53], we reported on high- to low- spin crossovers in putative d^8 insulating parent compounds of bilayer nickelates. Such crossovers occur as the ratio of Hund's coupling to interlayer superexchange between d_{z^2} spins is varied. A large J_H favors a spin-1 ground state (high spin) whereas a large interlayer superexchange favors a low-spin (*e.g.* spin 1/2) ground state. We argue that such high- to low- spin crossovers are also pertinent to the metallic $d^{7.5}$ configuration.

In the high-spin metallic state, magnetism is enhanced by a strong Hund's coupling, and interlayer superexchange is insufficient to forestall magnetism. With growing interlayer superexchange, superconducting correlations with Cooper pair formation across the bilayer start to grow. With further growth of interlayer superexchange, the Hund's coupling is not large enough to lock the d_{z^2} and $d_{x^2-y^2}$ orbital fluctuations and the d_{z^2} orbital forms a quantum disordered ground state comprised of interlayer singlets. The resulting low spin state can be thought of as weakly coupled layers each with a quarter filled $d_{x^2-y^2}$ band where the $d_{x^2-y^2}$ and d_{z^2} orbitals are nearly decoupled. In this regime, the in-plane pairing interaction dominates for $d_{x^2-y^2}$ orbitals, yielding a d -wave superconducting pairing symmetry with intralayer Cooper pair formation.

In Ref. [67], we provided evidence for this scenario by studying a model consisting of "local moments" in a half-filled d_{z^2} orbital coupled to quarter filled $d_{x^2-y^2}$ conduction electrons via a ferromagnetic "Kondo" coupling of strength J_H . In that work, we demonstrated that $(\pi/2, \pi/2)$ magnetism forms as a high-spin state stabilized by J_H . We also showed that interlayer Cooper pair formation occurs with increasing interlayer superexchange among d_{z^2} local moments. Our present RPA theory involves quite different underlying assumptions: both e_g orbitals are partially filled with sizeable charge and spin fluctuations. Nevertheless, the conclusions of the RPA theory are qualitatively similar to those of Ref. [67]. Large J_H favors $(\pi/2, \pi/2)$ magnetism. Superconductivity from repulsive interactions also favors gaps that change signs between the bonding and anti-bonding Fermi sheets. These solutions, when viewed in real space

consist of interlayer Cooper pair formation from $d_{x^2-y^2}$ electrons. As a result, J_H both stabilizes $(\pi/2, \pi/2)$ magnetism and drives the transition from d -wave to s_{\pm} -wave superconductivity.

In the real material, neither the local nor itinerant approach adequately captures the behavior of the microscopic degrees of freedom. Nevertheless, both frameworks make qualitatively similar predictions for magnetism and superconductivity. We therefore conclude that in this system, high temperature superconductivity likely develops along the crossover from high spin to low spin ground states.

ACKNOWLEDGMENTS

We thank Steven Kivelson, Bai Yang Wang, Jiarui Li and Hanbit Oh for useful discussions. Y.-M.W. acknowledges support from the Gordon and Betty Moore Foundation's EPiQS Initiative through GBMF8686. S.V.S. acknowledges the hospitality and support of the LITP Stanford. Y.-M.W., T.H. and S.R. are supported by the US Department of Energy, Office of Basic Energy Sciences, Division of Materials Sciences and Engineering, under Contract No. DE-AC02-76SF00515. S.V.S. was supported by the Hanns-Seidel Foundation and the Three Physicists Philanthropic Trust. T.H. was supported by the Deutsche Forschungsgemeinschaft (DFG, German Research Foundation) under Project No. 537357978.

Appendix A: Multiband RPA setup

We set up the kinetic model of the bilayer nickelates as the single-particle Hamiltonian defined in Eq. (2) of the main text. It is given by $H_0 = \sum_{\mathbf{k}, \sigma} \psi_{\sigma, \mathbf{k}}^\dagger \mathcal{H}_0(\mathbf{k}) \psi_{\sigma, \mathbf{k}}$ with $\psi_{\sigma, \mathbf{k}}^\dagger = (\psi_{X, \sigma, \mathbf{k}}^\dagger, \psi_{Z, \sigma, \mathbf{k}}^\dagger)$,

$$\mathcal{H}_0(\mathbf{k}) = \begin{pmatrix} \xi_X(\mathbf{k}) & T(\mathbf{k}) \\ T^\dagger(\mathbf{k}) & \xi_Z(\mathbf{k}) \end{pmatrix} \quad (\text{A1})$$

and matrix elements

$$\begin{aligned} \xi_X(\mathbf{k}) &= -2t_{1x} (\cos k_x + \cos k_y) - 4t_{2x} \cos k_x \cos k_y - \mu_d, \\ \xi_Z(\mathbf{k}) &= -t_z^\perp \cos \nu_c - 2t_{1z} (\cos k_x + \cos k_y) \\ &\quad - 4t_{2z} \cos k_x \cos k_y - \mu_f, \\ T(\mathbf{k}) &= -2t_{xz} (\cos k_x - \cos k_y) \\ &\quad - 2t_{xz}^\perp \cos \nu_c (\cos k_x - \cos k_y). \end{aligned} \quad (\text{A2})$$

Here, $\nu_c = 0, \pi$ corresponds to the bonding and anti-bonding band within the bilayer. The tight-binding parameters we use for the model are stated in Tab. I and are consistent with recent ARPES results [66]. For the interacting part H_I of the Hamiltonian, we use the

Parameter	Value (eV)
t_{1x}	0.345
t_{2x}	-0.057
μ_d	-0.851
t_{1z}	0.096
t_{2z}	0.051
t_z^\perp	0.42
μ_f	-0.192
t_{xz}	0.215
t_{xz}^\perp	-0.01

TABLE I. Model parameters for the tight-binding Hamiltonian in units of eV [66].

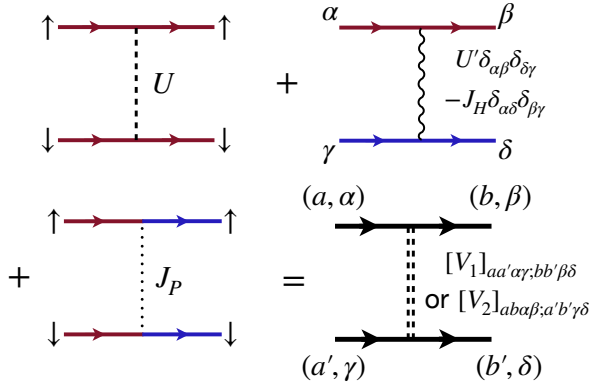


FIG. 5. Diagrammatic representation of the microscopic interactions considered in Eq. (A3). We use red and blue coloring to denote the $d_{x^2-y^2}$ and d_{z^2} orbitals respectively, while the spin indices are explicitly labeled. Depending on how the orbital and spin indices will be contracted, the total interaction can be equivalently written as V_1 or V_2 . Here, the black thick line denotes the matrix propagator including both orbitals.

Kanamori form as stated in Eq. (3) of the main text,

$$\begin{aligned}
H_I = & U \sum_{\ell, i, a} n_{a, \ell, i, \uparrow} n_{a, \ell, i, \downarrow} + U' \sum_{a \neq b, \ell, i, \sigma, \sigma'} n_{a, \ell, i, \sigma} n_{b, \ell, i, \sigma'} \\
& - J_H \sum_{\ell, i, \sigma, \sigma'} \psi_{X, \ell, i, \sigma}^\dagger \psi_{X, \ell, i, \sigma'} \psi_{Z, \ell, i, \sigma}^\dagger \psi_{Z, \ell, i, \sigma'} \\
& + J_P \sum_{\ell, i} \left(\psi_{X, \ell, i, \uparrow}^\dagger \psi_{X, \ell, i, \downarrow}^\dagger \psi_{Z, \ell, i, \downarrow} \psi_{Z, \ell, i, \uparrow} + h.c. \right).
\end{aligned} \tag{A3}$$

We fix $J_P = J_H$, but treat all remaining parameters as independent. The bare interactions of H_I are diagrammatically shown in Fig. 5. Note that both U' and the Hund's coupling J_H involve an interaction between the two orbitals, but their action in spin space is different.

In order to study the normal-state magnetic ordering as well as superconductive pairing instabilities, we employ the random phase approximation (RPA). In this method, we evaluate the geometric series of diagrams of

both transverse and longitudinal spin and orbital fluctuations. Such methods are standard and have shed considerable insight on unconventional pairing in a variety of materials [81]. Following Fig. 5, we label V_1 and V_2 as interactions arising from the transverse and longitudinal fluctuations, respectively. They correspond to different index contractions of the interaction (A3) written as either $[V_1]_{aa' \alpha \gamma; bb' \beta \delta}$ or $[V_2]_{aba \beta; a' b' \gamma \delta}$, where $aba'b'$ are orbital indices and $\alpha \beta \gamma \delta$ are spin indices. In this orbital-spin basis, both V_1 and V_2 are (16×16) -matrices, given by

$$\begin{aligned}
V_1 = & \begin{pmatrix} U & 0 & 0 & J_P \\ 0 & 0 & 0 & 0 \\ 0 & 0 & 0 & 0 \\ J_P & 0 & 0 & U \end{pmatrix} \otimes \begin{pmatrix} 0 & 0 & 0 & 0 \\ 0 & 1 & 0 & 0 \\ 0 & 0 & 1 & 0 \\ 0 & 0 & 0 & 0 \end{pmatrix} \\
& + \begin{pmatrix} 0 & 0 & 0 & 0 \\ 0 & 1 & 0 & 0 \\ 0 & 0 & 1 & 0 \\ 0 & 0 & 0 & 0 \end{pmatrix} \otimes \begin{pmatrix} U' - J_H & 0 & 0 & 0 \\ 0 & U' & -J_H & 0 \\ 0 & -J_H & U' & 0 \\ 0 & 0 & 0 & U' - J_H \end{pmatrix}
\end{aligned} \tag{A4}$$

and

$$\begin{aligned}
V_2 = & \begin{pmatrix} U & 0 & 0 & 0 \\ 0 & J_P & 0 & 0 \\ 0 & 0 & J_P & 0 \\ 0 & 0 & 0 & U \end{pmatrix} \otimes \begin{pmatrix} 0 & 0 & 0 & 1 \\ 0 & 0 & 0 & 0 \\ 0 & 0 & 0 & 0 \\ 1 & 0 & 0 & 0 \end{pmatrix} \\
& + \begin{pmatrix} 0 & 0 & 0 & 1 \\ 0 & 0 & 0 & 0 \\ 0 & 0 & 0 & 0 \\ 1 & 0 & 0 & 0 \end{pmatrix} \otimes \begin{pmatrix} U' - J_H & 0 & 0 & U' \\ 0 & 0 & -J_H & 0 \\ 0 & -J_H & 0 & 0 \\ U' & 0 & 0 & U' - J_H \end{pmatrix}.
\end{aligned} \tag{A5}$$

The building block of the geometric RPA series is the bare static polarization bubble which, in matrix form, is given by

$$\chi^0(\mathbf{q}) = - \int_k G_0(k) \otimes G_0(k + \mathbf{q}) \otimes \text{Id}_4. \tag{A6}$$

Here, $G_0(k) = [i\omega_n - \mathcal{H}_0(\mathbf{k})]^{-1}$ is the free matrix Green's function, Id_4 the (4×4) identity matrix in spin space and $\int_k \equiv \frac{T}{2} \sum_{\omega_n} \sum_{\nu_c=0, \pi} \int \frac{dk_x dk_y}{(2\pi)^2}$. We have used the abbreviation $k = (\omega_n, \mathbf{k})$ and $\omega_n = (2n + 1)\pi T$ is the fermionic Matsubara frequency.

We obtain the (16×16) -matrix form of the RPA susceptibility as the sum

$$\chi^{\text{RPA}}(\mathbf{q}) = \chi_1^{\text{RPA}}(\mathbf{q}) + \chi_2^{\text{RPA}}(\mathbf{q}), \tag{A7}$$

where the two terms $\chi_1^{\text{RPA}}(\mathbf{q})$ and $\chi_2^{\text{RPA}}(\mathbf{q})$ correspond to the transversal and longitudinal spin-orbital fluctuations respectively, similar to the pairing interaction in Fig. 6. They are given by

$$\chi_1^{\text{RPA}}(\mathbf{q}) = \chi^0(\mathbf{q}) (1 - V_1 \chi^0(\mathbf{q}))^{-1} \tag{A8}$$

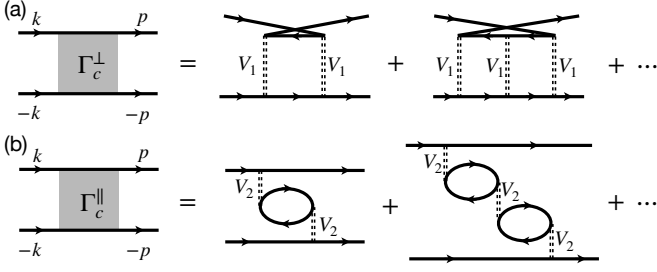


FIG. 6. Effective pairing interaction in the RPA scheme, which contains virtual processes of exchanging (a) transverse and (b) longitudinal spin-orbital fluctuations. The double dashed line is the tree-level interaction shown in Fig. 5.

and

$$\chi_2^{\text{RPA}}(\mathbf{q}) = -\chi^0(\mathbf{q})(1 + V_2\chi^0(\mathbf{q}))^{-1}. \quad (\text{A9})$$

Note that the first series is expressed in terms of V_1 , while the second one is expressed in terms of V_2 . For the superconducting instability, we then consider the following two geometric series that contribute to the total pairing vertex function Γ_c as shown in Fig. 6,

$$\Gamma_c^\perp(\mathbf{k}, \mathbf{p}) = V_1 \chi_1^{\text{RPA}}(\mathbf{k} + \mathbf{p}) V_1 \quad (\text{A10})$$

and

$$\Gamma_c^\parallel(\mathbf{k}, \mathbf{p}) = V_2 \chi_2^{\text{RPA}}(\mathbf{k} - \mathbf{p}) V_2. \quad (\text{A11})$$

Appendix B: Linearized gap equation

In the low energy limit, we consider the total spin $S_z = 0$ pairing configuration on the Fermi surface, and the effective pairing interaction in this channel is

$$\sum_{\mathbf{k}, \mathbf{p}} \sum_{aa', bb'} [V_{\text{eff}}(\mathbf{k}, \mathbf{p})]_{aa', bb'} \psi_{a, \uparrow, \mathbf{k}}^\dagger \psi_{a', \downarrow, \mathbf{k}}^\dagger \psi_{b', \downarrow, -\mathbf{k}} \psi_{b, \uparrow, -\mathbf{p}}, \quad (\text{B1})$$

where

$$[V_{\text{eff}}(\mathbf{k}, \mathbf{p})]_{aa', bb'} = [V_1 + \Gamma_c^\perp(\mathbf{k}, \mathbf{p})]_{aa' \uparrow \downarrow, bb' \uparrow \downarrow} + [\Gamma_c^\parallel(\mathbf{k}, \mathbf{p})]_{ab \uparrow \downarrow, a' b' \downarrow \uparrow} \quad (\text{B2})$$

and both \mathbf{k} and \mathbf{p} are on the Fermi surface. In our RPA analysis, we explicitly include the bare (tree-level) interaction term in the pairing vertex, as this contribution becomes important whenever a conventional s -wave pairing channel competes with fluctuation-mediated pairings. The most general form of the superconducting order parameter is written as

$$\hat{\Delta}(\mathbf{k}) = \sum_{i=1}^4 \Delta_i(\mathbf{k}) \Gamma^i = \begin{pmatrix} \Delta_{XX}(\mathbf{k}) & \Delta_{XZ}(\mathbf{k}) \\ \Delta_{ZX}(\mathbf{k}) & \Delta_{ZZ}(\mathbf{k}) \end{pmatrix} \quad (\text{B3})$$

with

$$\Gamma^1 = \begin{pmatrix} 1 & 0 \\ 0 & 0 \end{pmatrix}, \Gamma^2 = \begin{pmatrix} 0 & 1 \\ 0 & 0 \end{pmatrix}, \Gamma^3 = \begin{pmatrix} 0 & 0 \\ 1 & 0 \end{pmatrix}, \Gamma^4 = \begin{pmatrix} 0 & 0 \\ 0 & 1 \end{pmatrix}.$$

Therefore we identify $\Delta_1(\mathbf{k}) = \Delta_{XX}(\mathbf{k})$, $\Delta_2(\mathbf{k}) = \Delta_{XZ}(\mathbf{k})$, $\Delta_3(\mathbf{k}) = \Delta_{ZX}(\mathbf{k})$ and $\Delta_4(\mathbf{k}) = \Delta_{ZZ}(\mathbf{k})$. The subscripts are chosen to encode the orbital information, e.g. Δ_{XX} is the pairing gap within the $d_{x^2-y^2}$ orbitals. The linearized gap equation from the effective pairing interaction on the Fermi surface is given by

$$\Delta_i(\mathbf{k}) = -\frac{1}{N_{\text{FS}}} \sum_{\mathbf{p} \in \text{FS}} \sum_{j, l=1}^4 [V_{\text{eff}}(\mathbf{k}, \mathbf{p})]_{i, j} P^{j, l}(\mathbf{p}) \Delta_l(\mathbf{p}), \quad (\text{B4})$$

N_{FS} is the number of sampled momentum points on the FS. The particle-particle polarization matrix $P(\mathbf{p})$ is given by $P^{j, l}(\mathbf{p}) = \text{Tr} \left[\frac{T}{N_\perp} \sum_{\mathbf{p}_\perp, \omega_n} G_0(-\mathbf{p}) \Gamma^j G_0(\mathbf{p}) \Gamma^l \right]$ where $\mathbf{p} = (\omega_n, \mathbf{p}, \mathbf{p}_\perp)$ and \mathbf{p}_\perp denotes N_\perp momentum points along the direction perpendicular to the FS at \mathbf{p} . Therefore, the leading pairing symmetry can be found by diagonalizing the symmetrized kernel [86–88]

$$g_{\mathbf{k}, \mathbf{p}} = \frac{1}{N_{\text{FS}}} P^{\frac{1}{2}}(\mathbf{k}) V_{\text{eff}}(\mathbf{k}, \mathbf{p}) P^{\frac{1}{2}}(\mathbf{p}) \quad (\text{B5})$$

and identifying the dominant pairing channel as the most negative eigenvalue of (B5). For that, we use a discretization of 150 points in each of the α, β Fermi surface pockets and obtain the static susceptibility $\chi^0(\mathbf{q})$ in the $T \rightarrow 0$ limit on a discretized 100×100 mesh of the BZ. The pair wave function is then given by the eigenvector associated to the dominant pairing strength. Since the gap function in Eq. (B3) is defined in terms of the orbital basis, we similarity transform it to the band basis.

Assuming it is the j -th band that is on the Fermi surface at each $\mathbf{k} \in \text{FS}$, the band basis projected gap function is given by

$$\Delta(\mathbf{k}) = \sum_{a, a'} u_{a, j}^*(\mathbf{k}) \Delta_{aa'}(\mathbf{k}) u_{a', j}^*(-\mathbf{k}) \quad (\text{B6})$$

where $a, a' \in (X, Z)$ and $u_{X, j}^*(\mathbf{k})$, $u_{Z, j}^*(\mathbf{k})$ are the complex conjugated components of the eigenvector of the j -th band of $\mathcal{H}_0(\mathbf{k})$. Given that the bands of $\mathcal{H}_0(\mathbf{k})$ are topologically trivial, we choose the projected gap function $\Delta(\mathbf{k})$ to be real.

Appendix C: RPA spin susceptibility

As discussed in the main text, we consider the bare total spin susceptibility which is obtained by summing over the orbital indices of the bare susceptibility $\chi^0(\mathbf{q})$ (defined in Appendix A) as

$$\chi_S^0(\mathbf{q}) = \sum_{a, b} [\chi^0(\mathbf{q})]_{aa, bb}. \quad (\text{C1})$$

The full RPA total spin- S_z susceptibility is then obtained by

$$\chi_S^{\text{RPA}}(\mathbf{q}) = \sum_{a, b} \sum_{\alpha\gamma\beta\delta} [\chi^{\text{RPA}}(\mathbf{q})]_{aa\alpha\gamma; bb\beta\delta} \sigma_{\alpha\gamma}^z \sigma_{\beta\delta}^z, \quad (\text{C2})$$

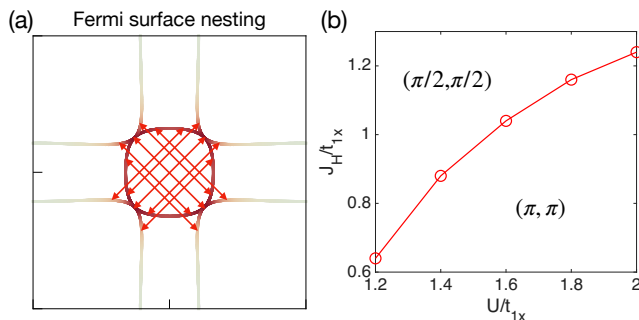


FIG. 7. (a) Fermi surface nesting of momenta close to $(\pi/2, \pi/2)$, as visible in the bare total spin susceptibility $\chi_S^0(\mathbf{q})$ in Fig. 4 of the main text. (b) Separation between the dominant (π, π) and $(\pi/2, \pi/2)$ spin fluctuations, determined by the maximum position of the RPA total spin susceptibility $\chi_S^{\text{RPA}}(\mathbf{q})$ in Fig. 4 of the main text.

where a, b are orbital indices and $\alpha, \beta, \gamma, \delta$ are spin indices. In Fig. 7(a) we show nesting effects within the Fermi surface with the red arrows being momentum, measured by the peak positions in $\chi_S^0(\mathbf{q})$, as plotted in Fig. 4 of the main text. Since we implicitly keep $\nu_c = \pi$, the momenta have to connect α -FS to β -FS and vice versa. Although not perfect, the nesting effect can still be seen from the figure which mainly occurs between $d_{x^2-y^2}$ orbitals.

In the main text, we discussed the competition between a $(\pi/2, \pi/2)$ and a (π, π) SDW order. In Fig. 7(b) we present the boundary between the two spin orders in the J_H - U plane by keeping $U' = t_{1x}$. We note that our weak coupling theory here suggest that the critical J_H needed to induce the near $(\pi/2, \pi/2)$ order *increases* with increasing U . This is opposite to the result of the strong coupling limit [67].

- [1] H. Sun, M. Huo, X. Hu, J. Li, Z. Liu, Y. Han, L. Tang, Z. Mao, P. Yang, B. Wang, J. Cheng, D.-X. Yao, G.-M. Zhang, and M. Wang, Signatures of superconductivity near 80 k in a nickelate under high pressure, *Nature* **621**, 493 (2023).
- [2] Y. Zhang, D. Su, Y. Huang, Z. Shan, H. Sun, M. Huo, K. Ye, J. Zhang, Z. Yang, Y. Xu, Y. Su, R. Li, M. Smidman, M. Wang, L. Jiao, and H. Yuan, High-temperature superconductivity with zero-resistance and strange metal behavior in $\text{La}_3\text{Ni}_2\text{O}_{7-\delta}$, *Nature Physics* **20**, 1269 (2024).
- [3] J. Hou, P.-T. Yang, Z.-Y. Liu, J.-Y. Li, P.-F. Shan, L. Ma, G. Wang, N.-N. Wang, H.-Z. Guo, J.-P. Sun, Y. Uwatoko, M. Wang, G.-M. Zhang, B.-S. Wang, and J.-G. Cheng, Emergence of High-Temperature Superconducting Phase in Pressurized $\text{La}_3\text{Ni}_2\text{O}_7$ Crystals, *Chinese Physics Letters* **40**, 117302 (2023).
- [4] Z. Liu, M. Huo, J. Li, Q. Li, Y. Liu, Y. Dai, X. Zhou, J. Hao, Y. Lu, M. Wang, and H.-H. Wen, Electronic correlations and partial gap in the bilayer nickelate $\text{La}_3\text{Ni}_2\text{O}_7$, *Nature Communications* **15**, 7570 (2024).
- [5] J. Yang, H. Sun, X. Hu, Y. Xie, T. Miao, H. Luo, H. Chen, B. Liang, W. Zhu, G. Qu, C.-Q. Chen, M. Huo, Y. Huang, S. Zhang, F. Zhang, F. Yang, Z. Wang, Q. Peng, H. Mao, G. Liu, Z. Xu, T. Qian, D.-X. Yao, M. Wang, L. Zhao, and X. J. Zhou, Orbital-dependent electron correlation in double-layer nickelate $\text{La}_3\text{Ni}_2\text{O}_7$, *Nature Communications* **15**, 4373 (2024).
- [6] M. Zhang, C. Pei, Q. Wang, Y. Zhao, C. Li, W. Cao, S. Zhu, J. Wu, and Y. Qi, Effects of pressure and doping on Ruddlesden-Popper phases $\text{La}_{n+1}\text{Ni}_n\text{O}_{3n+1}$, *Journal of Materials Science & Technology* **185**, 147 (2024).
- [7] E. K. Ko, Y. Yu, Y. Liu, L. Bhatt, J. Li, V. Thampy, C.-T. Kuo, B. Y. Wang, Y. Lee, K. Lee, J.-S. Lee, B. H. Goodge, D. A. Muller, and H. Y. Hwang, Signatures of ambient pressure superconductivity in thin film $\text{La}_3\text{Ni}_2\text{O}_7$, *Nature* [10.1038/s41586-024-08525-3](https://doi.org/10.1038/s41586-024-08525-3) (2024).
- [8] G. Zhou, W. Lv, H. Wang, Z. Nie, Y. Chen, Y. Li, H. Huang, W.-Q. Chen, Y.-J. Sun, Q.-K. Xue, and Z. Chen, Ambient-pressure superconductivity onset above 40 K in $(\text{La,Pr})_3\text{Ni}_2\text{O}_7$ films, *Nature* **640**, 641 (2025).
- [9] Y. Liu, E. K. Ko, Y. Tarn, L. Bhatt, J. Li, V. Thampy, B. H. Goodge, D. A. Muller, S. Raghu, Y. Yu, and H. Y. Hwang, Superconductivity and normal-state transport in compressively strained $\text{La}_2\text{PrNi}_2\text{O}_7$ thin films, *Nature Materials* **24**, 1221 (2025).
- [10] L. Wang, Y. Li, S.-Y. Xie, F. Liu, H. Sun, C. Huang, Y. Gao, T. Nakagawa, B. Fu, B. Dong, Z. Cao, R. Yu, S. I. Kawaguchi, H. Kadobayashi, M. Wang, C. Jin, H.-k. Mao, and H. Liu, Structure Responsible for the Superconducting State in $\text{La}_3\text{Ni}_2\text{O}_7$ at High-Pressure and Low-Temperature Conditions, *Journal of the American Chemical Society* **146**, 7506 (2024).
- [11] L. Bhatt, A. Y. Jiang, E. K. Ko, N. Schnitzer, G. A. Pan, D. F. Segedin, Y. Liu, Y. Yu, Y.-F. Zhao, E. A. Morales, C. M. Brooks, A. S. Botana, H. Y. Hwang, J. A. Mundy, D. A. Muller, and B. H. Goodge, Resolving structural origins for superconductivity in strain-engineered $\text{la}_3\text{ni}_2\text{o}_7$ thin films (2025), [arXiv:2501.08204 \[cond-mat.supr-con\]](https://arxiv.org/abs/2501.08204).
- [12] X. Chen, J. Choi, Z. Jiang, J. Mei, K. Jiang, J. Li, S. Agrestini, M. Garcia-Fernandez, H. Sun, X. Huang, D. Shen, M. Wang, J. Hu, Y. Lu, K.-J. Zhou, and D. Feng, Electronic and magnetic excitations in $\text{La}_3\text{Ni}_2\text{O}_7$, *Nature Communications* **15**, 9597 (2024).
- [13] K. Chen, X. Liu, J. Jiao, M. Zou, C. Jiang, X. Li, Y. Luo, Q. Wu, N. Zhang, Y. Guo, and L. Shu, Evidence of Spin Density Waves in $\text{La}_3\text{Ni}_2\text{O}_{7-\delta}$, *Phys. Rev. Lett.* **132**, 256503 (2024).
- [14] R. Khasanov, T. J. Hicken, D. J. Gawryluk, V. Sazgari, I. Plokhikh, L. P. Sorel, M. Bartkowiak, S. Bötzel, F. Lechermann, I. M. Eremin, H. Luetkens, and Z. Guguchia, Pressure-enhanced splitting of density wave transitions in $\text{La}_3\text{Ni}_2\text{O}_{7-\delta}$, *Nature Physics* **21**, 430 (2025).
- [15] D. Zhao, Y. Zhou, M. Huo, Y. Wang, L. Nie, Y. Yang, J. Ying, M. Wang, T. Wu, and X. Chen, Pressure-enhanced spin-density-wave transition in double-layer nickelate $\text{La}_3\text{Ni}_2\text{O}_{7-\delta}$, *Science Bulletin* **70**, 1239 (2025).
- [16] M. Kakoi, T. Oi, Y. Ohshita, M. Yashima, K. Kuroki, T. Kato, H. Takahashi, S. Ishiwata, Y. Adachi, N. Hatada, *et al.*, Multiband metallic ground state in multilayered nickelates $\text{La}_3\text{Ni}_2\text{O}_7$ and $\text{La}_4\text{Ni}_3\text{O}_{10}$ probed

- by ^{139}La -NMR at ambient pressure, *Journal of the Physical Society of Japan* **93**, 053702 (2024).
- [17] T. Xie, M. Huo, X. Ni, F. Shen, X. Huang, H. Sun, H. C. Walker, D. Adroja, D. Yu, B. Shen, L. He, K. Cao, and M. Wang, Strong interlayer magnetic exchange coupling in $\text{La}_3\text{Ni}_2\text{O}_{7-\delta}$ revealed by inelastic neutron scattering, *Science Bulletin* **69**, 3221 (2024).
- [18] N. K. Gupta, R. Gong, Y. Wu, M. Kang, C. T. Parzyck, B. Z. Gregory, N. Costa, R. Sutarto, S. Sarker, A. Singer, D. G. Schlom, K. M. Shen, and D. G. Hawthorn, Anisotropic spin stripe domains in bilayer $\text{La}_3\text{Ni}_2\text{O}_7$, *Nature Communications* **16**, 6560 (2025).
- [19] X. Ren, R. Sutarto, X. Wu, J. Zhang, H. Huang, T. Xiang, J. Hu, R. Comin, X. Zhou, and Z. Zhu, Resolving the electronic ground state of $\text{La}_3\text{Ni}_2\text{O}_{7-\delta}$ films, *Communications Physics* **8**, 52 (2025).
- [20] G. Shirane, Y. Endoh, R. J. Birgeneau, M. A. Kastner, Y. Hidaka, M. Oda, M. Suzuki, and T. Murakami, Two-dimensional antiferromagnetic quantum spin-fluid state in La_2CuO_4 , *Phys. Rev. Lett.* **59**, 1613 (1987).
- [21] Y. Endoh, K. Yamada, R. J. Birgeneau, D. R. Gabbe, H. P. Jenssen, M. A. Kastner, C. J. Peters, P. J. Picone, T. R. Thurston, J. M. Tranquada, G. Shirane, Y. Hidaka, M. Oda, Y. Enomoto, M. Suzuki, and T. Murakami, Static and dynamic spin correlations in pure and doped La_2CuO_4 , *Phys. Rev. B* **37**, 7443 (1988).
- [22] Q.-G. Yang, D. Wang, and Q.-H. Wang, Possible s_{\pm} -wave superconductivity in $\text{La}_3\text{Ni}_2\text{O}_7$, *Phys. Rev. B* **108**, L140505 (2023).
- [23] Y.-f. Yang, G.-M. Zhang, and F.-C. Zhang, Interlayer valence bonds and two-component theory for high- T_c superconductivity of $\text{La}_3\text{Ni}_2\text{O}_7$ under pressure, *Phys. Rev. B* **108**, L201108 (2023).
- [24] C. Lu, Z. Pan, F. Yang, and C. Wu, Interlayer-Coupling-Driven High-Temperature Superconductivity in $\text{La}_3\text{Ni}_2\text{O}_7$ under Pressure, *Phys. Rev. Lett.* **132**, 146002 (2024).
- [25] X.-Z. Qu, D.-W. Qu, J. Chen, C. Wu, F. Yang, W. Li, and G. Su, Bilayer $t-J-J_{\perp}$ Model and Magnetically Mediated Pairing in the Pressurized Nickelate $\text{La}_3\text{Ni}_2\text{O}_7$, *Phys. Rev. Lett.* **132**, 036502 (2024).
- [26] H. Oh and Y.-H. Zhang, Type-II $t-J$ model and shared superexchange coupling from Hund's rule in superconducting $\text{La}_3\text{Ni}_2\text{O}_7$, *Phys. Rev. B* **108**, 174511 (2023).
- [27] H. Yang, H. Oh, and Y.-H. Zhang, Strong pairing from a small Fermi surface beyond weak coupling: Application to $\text{La}_3\text{Ni}_2\text{O}_7$, *Phys. Rev. B* **110**, 104517 (2024).
- [28] Z. Luo, X. Hu, M. Wang, W. Wú, and D.-X. Yao, Bilayer two-orbital model of $\text{La}_3\text{Ni}_2\text{O}_7$ under pressure, *Phys. Rev. Lett.* **131**, 126001 (2023).
- [29] Y. Gu, C. Le, Z. Yang, X. Wu, and J. Hu, Effective model and pairing tendency in the bilayer Ni-based superconductor $\text{La}_3\text{Ni}_2\text{O}_7$, *Phys. Rev. B* **111**, 174506 (2025).
- [30] Y. Shen, M. Qin, and G.-M. Zhang, Effective bi-layer model Hamiltonian and density-matrix renormalization group study for the high- T_c superconductivity in $\text{La}_3\text{Ni}_2\text{O}_7$ under high pressure, *Chinese Physics Letters* **40**, 127401 (2023).
- [31] H. Oh, B. Zhou, and Y.-H. Zhang, Type-II $t-J$ model in charge transfer regime in bilayer $\text{La}_3\text{Ni}_2\text{O}_7$ and trilayer $\text{La}_4\text{Ni}_3\text{O}_{10}$, *Phys. Rev. B* **111**, L020504 (2025).
- [32] V. Christiansson, F. Petocchi, and P. Werner, Correlated Electronic Structure of $\text{La}_3\text{Ni}_2\text{O}_7$ under Pressure, *Phys. Rev. Lett.* **131**, 206501 (2023).
- [33] Y.-B. Liu, J.-W. Mei, F. Ye, W.-Q. Chen, and F. Yang, s_{\pm} -Wave Pairing and the Destructive Role of Apical-Oxygen Deficiencies in $\text{La}_3\text{Ni}_2\text{O}_7$ under Pressure, *Phys. Rev. Lett.* **131**, 236002 (2023).
- [34] Y. Cao and Y.-f. Yang, Flat bands promoted by Hund's rule coupling in the candidate double-layer high-temperature superconductor $\text{La}_3\text{Ni}_2\text{O}_7$ under high pressure, *Phys. Rev. B* **109**, L081105 (2024).
- [35] D.-C. Lu, M. Li, Z.-Y. Zeng, W. Hou, J. Wang, F. Yang, and Y.-Z. You, Superconductivity from Doping Symmetric Mass Generation Insulators: Application to $\text{La}_3\text{Ni}_2\text{O}_7$ under Pressure, arXiv preprint arXiv:2308.11195 (2023).
- [36] R. Jiang, J. Hou, Z. Fan, Z.-J. Lang, and W. Ku, Pressure Driven Fractionalization of Ionic Spins Results in Cupratelike High- T_c Superconductivity in $\text{La}_3\text{Ni}_2\text{O}_7$, *Phys. Rev. Lett.* **132**, 126503 (2024).
- [37] Y.-H. Tian, Y. Chen, J.-M. Wang, R.-Q. He, and Z.-Y. Lu, Correlation effects and concomitant two-orbital s_{\pm} -wave superconductivity in $\text{La}_3\text{Ni}_2\text{O}_7$ under high pressure, *Phys. Rev. B* **109**, 165154 (2024).
- [38] J.-X. Zhang, H.-K. Zhang, Y.-Z. You, and Z.-Y. Weng, Strong Pairing Originated from an Emergent \mathbb{Z}_2 Berry Phase in $\text{La}_3\text{Ni}_2\text{O}_7$, *Phys. Rev. Lett.* **133**, 126501 (2024).
- [39] Q. Qin and Y.-f. Yang, High- T_c superconductivity by mobilizing local spin singlets and possible route to higher T_c in pressurized $\text{La}_3\text{Ni}_2\text{O}_7$, *Phys. Rev. B* **108**, L140504 (2023).
- [40] J. Huang, Z. D. Wang, and T. Zhou, Impurity and vortex states in the bilayer high-temperature superconductor $\text{La}_3\text{Ni}_2\text{O}_7$, *Phys. Rev. B* **108**, 174501 (2023).
- [41] N. Kitamine, M. Ochi, and K. Kuroki, Theoretical designing of multiband Nickelate and Palladate superconductors with $d^{8+\delta}$ configuration, arXiv e-prints, arXiv:2308.12750 (2023), arXiv:2308.12750 [cond-mat.supr-con].
- [42] H. Lange, L. Homeier, E. Demler, U. Schollwöck, A. Bohrdt, and F. Grusdt, Pairing dome from an emergent feshbach resonance in a strongly repulsive bilayer model, *Phys. Rev. B* **110**, L081113 (2024).
- [43] H. Lange, L. Homeier, E. Demler, U. Schollwöck, F. Grusdt, and A. Bohrdt, Feshbach resonance in a strongly repulsive bilayer model: a possible scenario for bilayer nickelate superconductors (2023), arXiv:2309.15843 [cond-mat.str-el].
- [44] H. Schlömer, U. Schollwöck, F. Grusdt, and A. Bohrdt, Superconductivity in the pressurized nickelate $\text{La}_3\text{Ni}_2\text{O}_7$ in the vicinity of a BEC-BCS crossover (2023), arXiv:2311.03349 [cond-mat.str-el].
- [45] J. Zhan, Y. Gu, X. Wu, and J. Hu, Cooperation between electron-phonon coupling and electronic interaction in bilayer nickelates $\text{La}_3\text{Ni}_2\text{O}_7$ (2024), arXiv:2404.03638 [cond-mat.supr-con].
- [46] F. Lechermann, S. Bötzel, and I. M. Eremin, Electronic instability, layer selectivity, and Fermi arcs in $\text{La}_3\text{Ni}_2\text{O}_7$, *Phys. Rev. Mater.* **8**, 074802 (2024).
- [47] G. Wang, N. Wang, X. Shen, J. Hou, L. Ma, L. Shi, Z. Ren, Y. Gu, H. Ma, P. Yang, *et al.*, Pressure-induced superconductivity in polycrystalline $\text{La}_3\text{Ni}_2\text{O}_{7-\delta}$, *Physical Review X* **14**, 011040 (2024).
- [48] J.-R. Xue and F. Wang, Magnetism and Superconductivity in the t - J Model of $\text{La}_3\text{Ni}_2\text{O}_7$ Under Multiband Gutzwiller Approximation, *Chinese Physics Letters* **41**, 057403 (2024).
- [49] Y. Zhang, L.-F. Lin, A. Moreo, T. A. Maier, and

- E. Dagotto, Structural phase transition, s_{\pm} -wave pairing, and magnetic stripe order in bilayered superconductor $\text{La}_3\text{Ni}_2\text{O}_7$ under pressure, *Nature Communications* **15**, 2470 (2024).
- [50] Y. Zhang, L.-F. Lin, A. Moreo, T. A. Maier, and E. Dagotto, Trends in electronic structures and s_{\pm} -wave pairing for the rare-earth series in bilayer nickelate superconductor $R_3\text{Ni}_2\text{O}_7$, *Phys. Rev. B* **108**, 165141 (2023).
- [51] K. Jiang, Z. Wang, and F.-C. Zhang, High-temperature superconductivity in $\text{La}_3\text{Ni}_2\text{O}_7$, *Chinese Physics Letters* **41**, 017402 (2024).
- [52] Z. Liao, L. Chen, G. Duan, Y. Wang, C. Liu, R. Yu, and Q. Si, Electron correlations and superconductivity in $\text{La}_3\text{Ni}_2\text{O}_7$ under pressure tuning, *Phys. Rev. B* **108**, 214522 (2023).
- [53] H. Oh, Y.-M. Wu, J. May-Mann, Y. Yu, H. Y. Hwang, Y.-H. Zhang, and S. Raghu, High spin, low spin or gapped spins: magnetism in the bilayer nickelates (2025), arXiv:2506.18973 [cond-mat.str-el].
- [54] B. Geisler, L. Fanfarillo, J. J. Hamlin, G. R. Stewart, R. G. Hennig, and P. J. Hirschfeld, Optical properties and electronic correlations in $\text{La}_3\text{Ni}_2\text{O}_7$ bilayer nickelates under high pressure, *npj Quantum Materials* **9**, 89 (2024).
- [55] B. Geisler, J. J. Hamlin, G. R. Stewart, R. G. Hennig, and P. J. Hirschfeld, Electronic reconstruction and interface engineering of emergent spin fluctuations in compressively strained $\text{La}_3\text{Ni}_2\text{O}_7$ on $\text{SrLaAlO}_4(001)$ (2025), arXiv:2503.10902 [cond-mat.supr-con].
- [56] G. Khalilullin and J. Chaloupka, Orbital order and superconductivity in bilayer nickelate compounds (2025), arXiv:2506.16360 [cond-mat.str-el].
- [57] H. Oh, H. Yang, and Y.-H. Zhang, Doping a spin-one mott insulator: possible application to bilayer nickelate (2025), arXiv:2509.02673 [cond-mat.str-el].
- [58] H. Yang, H. Oh, and Y.-H. Zhang, Strong pairing and symmetric pseudogap metal in a double kondo lattice model: From a nickelate superconductor to a tetralayer optical lattice, *Phys. Rev. B* **111**, L241102 (2025).
- [59] Y. Zhang, L.-F. Lin, A. Moreo, and E. Dagotto, Electronic structure, dimer physics, orbital-selective behavior, and magnetic tendencies in the bilayer nickelate superconductor $\text{La}_3\text{Ni}_2\text{O}_7$ under pressure, *Phys. Rev. B* **108**, L180510 (2023).
- [60] C. Lu, Z. Pan, F. Yang, and C. Wu, Interplay of two E_g orbitals in superconducting $\text{La}_3\text{Ni}_2\text{O}_7$ under pressure, *Phys. Rev. B* **110**, 094509 (2024).
- [61] X. Zhu, W. Qin, P. Cui, and Z. Zhang, Quantum phase transition driven by competing intralayer and interlayer hopping of $\text{ni-}d_{3z^2-r^2}$ orbitals in bilayer nickelates (2025), arXiv:2507.11169 [cond-mat.str-el].
- [62] Y. Zhang, L.-F. Lin, A. Moreo, T. A. Maier, and E. Dagotto, Electronic structure, self-doping, and superconducting instability in the alternating single-layer trilayer stacking nickelates $\text{La}_3\text{Ni}_2\text{O}_7$, *Phys. Rev. B* **110**, L060510 (2024).
- [63] S. Ryeong, N. Witt, G. Sangiovanni, and T. O. Wehling, Superconductivity governed by janus-faced fermiology in strained bilayer nickelates, *Phys. Rev. Lett.* **135**, 236003 (2025).
- [64] P. Li, G. Zhou, W. Lv, Y. Li, C. Yue, H. Huang, L. Xu, J. Shen, Y. Miao, W. Song, Z. Nie, Y. Chen, H. Wang, W. Chen, Y. Huang, Z.-H. Chen, T. Qian, J. Lin, J. He, Y.-J. Sun, Z. Chen, and Q.-K. Xue, Angle-resolved photoemission spectroscopy of superconducting $(\text{La},\text{Pr})_3\text{Ni}_2\text{O}_7/\text{SrLaAlO}_4$ heterostructures, *National Science Review* **10.1093/nsr/nwaf205** (2025).
- [65] C. Yue, J.-J. Miao, H. Huang, Y. Hua, P. Li, Y. Li, G. Zhou, W. Lv, Q. Yang, H. Sun, Y.-J. Sun, J. Lin, Q.-K. Xue, Z. Chen, and W.-Q. Chen, Correlated electronic structures and unconventional superconductivity in bilayer nickelate heterostructures (2025), arXiv:2501.06875 [cond-mat.str-el].
- [66] B. Y. Wang, Y. Zhong, S. Abadi, Y. Liu, Y. Yu, X. Zhang, Y.-M. Wu, R. Wang, J. Li, Y. Tarn, E. K. Ko, V. Thampy, M. Hashimoto, D. Lu, Y. S. Lee, T. P. Devereaux, C. Jia, H. Y. Hwang, and Z.-X. Shen, Electronic structure of compressively strained thin film $\text{La}_2\text{PrNi}_2\text{O}_7$ (2025), arXiv:2504.16372 [cond-mat.supr-con].
- [67] H.-X. Wang, H. Oh, T. Helbig, B. Y. Wang, J. Li, Y. Yu, H. Y. Hwang, H.-C. Jiang, Y.-M. Wu, and S. Raghu, Origin of Spin Stripes in Bilayer Nickelate $\text{La}_3\text{Ni}_2\text{O}_7$ (2025), arXiv:2509.25344 [cond-mat.supr-con].
- [68] S. Fan, M. Ou, M. Scholten, Q. Li, Z. Shang, Y. Wang, J. Xu, H. Yang, I. M. Eremin, and H.-H. Wen, Superconducting gap structure and bosonic mode in $\text{La}_2\text{PrNi}_2\text{O}_7$ thin films at ambient pressure (2025), arXiv:2506.01788 [cond-mat.supr-con].
- [69] J. Guo, Y. Chen, Y. Wang, H. Sun, D. Hu, M. Wang, X. Huang, and T. Cui, Revealing superconducting gap in $\text{La}_3\text{Ni}_2\text{O}_7-\delta$ by andreev reflection spectroscopy under high pressure (2025), arXiv:2509.12601 [cond-mat.supr-con].
- [70] Z.-Y. Cao, D. Peng, S. Choi, F. Lan, L. Yu, E. Zhang, Z. Xing, Y. Liu, F. Zhang, T. Luo, L. Chen, V. T. A. Hong, S.-Y. Paek, H. Jang, J. Xie, H. Liu, H. Lou, Z. Zeng, Y. Ding, J. Zhao, C. Liu, T. Park, Q. Zeng, and H. Kwang Mao, Direct observation of d-wave superconducting gap symmetry in pressurized $\text{La}_3\text{Ni}_2\text{O}_7$ -delta single crystals (2025), arXiv:2509.12606 [cond-mat.supr-con].
- [71] T. A. Maier and D. J. Scalapino, Pair structure and the pairing interaction in a bilayer hubbard model for unconventional superconductivity, *Phys. Rev. B* **84**, 180513 (2011).
- [72] K.-Y. Jiang, Y.-H. Cao, Q.-G. Yang, H.-Y. Lu, and Q.-H. Wang, Theory of Pressure Dependence of Superconductivity in Bilayer Nickelate $\text{La}_3\text{Ni}_2\text{O}_7$, *Phys. Rev. Lett.* **134**, 076001 (2025).
- [73] S. Ryeong, N. Witt, and T. O. Wehling, Quenched pair breaking by interlayer correlations as a key to superconductivity in $\text{La}_3\text{Ni}_2\text{O}_7$, *Phys. Rev. Lett.* **133**, 096002 (2024).
- [74] Y.-Y. Zheng and W. Wú, s_{\pm} -wave superconductivity in the bilayer two-orbital Hubbard model, *Phys. Rev. B* **111**, 035108 (2025).
- [75] Z. Luo, B. Lv, M. Wang, W. Wú, and D.-X. Yao, High-TC superconductivity in $\text{La}_3\text{Ni}_2\text{O}_7$ based on the bilayer two-orbital t-J model, *npj Quantum Materials* **9**, 61 (2024).
- [76] H. Sakakibara, N. Kitamine, M. Ochi, and K. Kuroki, Possible High T_c Superconductivity in $\text{La}_3\text{Ni}_2\text{O}_7$ under High Pressure through Manifestation of a Nearly Half-Filled Bilayer Hubbard Model, *Phys. Rev. Lett.* **132**, 106002 (2024).
- [77] K. Jiang, Z. Wang, and F.-C. Zhang, High-Temperature Superconductivity in $\text{La}_3\text{Ni}_2\text{O}_7$, *Chinese Physics Letters* **41**, 017402 (2024).
- [78] N. F. Berk and J. R. Schrieffer, Effect of ferromagnetic spin correlations on superconductivity, *Phys. Rev. Lett.*

- [17](#), [433](#) (1966).
- [79] D. Scalapino, The case for $d_{x^2-y^2}$ pairing in the cuprate superconductors, [Physics Reports](#) **250**, [329](#) (1995).
- [80] T. Maier, T. Berlijn, and D. J. Scalapino, Two pairing domes as Cu^{2+} varies to Cu^{3+} , [Phys. Rev. B](#) **99**, [224515](#) (2019).
- [81] D. J. Scalapino, A common thread: The pairing interaction for unconventional superconductors, [Rev. Mod. Phys.](#) **84**, [1383](#) (2012).
- [82] J. Kanamori, Electron correlation and ferromagnetism of transition metals, [Progress of Theoretical Physics](#) **30**, [275](#) (1963).
- [83] A. Georges, L. d. Medici, and J. Mravlje, Strong correlations from hund's coupling, [Annual Review of Condensed Matter Physics](#) **4**, [137](#) (2013).
- [84] D. I. Khomskii, *Transition metal compounds* (Cambridge University Press, 2014).
- [85] See Ref. [79] for the definition of transverse and longitudinal spin fluctuations.
- [86] S. Raghu, S. A. Kivelson, and D. J. Scalapino, Superconductivity in the repulsive hubbard model: An asymptotically exact weak-coupling solution, [Phys. Rev. B](#) **81**, [224505](#) (2010).
- [87] W. Cho, R. Thomale, S. Raghu, and S. A. Kivelson, Band structure effects on the superconductivity in hubbard models, [Phys. Rev. B](#) **88**, [064505](#) (2013).
- [88] Y.-M. Wu, Z. Wu, and H. Yao, Pair-density-wave and chiral superconductivity in twisted bilayer transition metal dichalcogenides, [Phys. Rev. Lett.](#) **130**, [126001](#) (2023).